Original Article

JHSMR Journal of Health Science and Medical Research

Magnetic Resonance Imaging in Evaluation of Bone Tumor Matrix: Diagnostic Value and Matrix Characteristics

Wisitsak Pakdee, M.D.[1], Warunee Kaewpiboon, M.D.[1], Teeranan Laohawiriyakamol, M.D.[1], Pattira Boonsri, M.D.[1], Khanin Iamthanaporn, M.D.[2], Pramot Tanutit, M.D.[1]

[1]Department of Radiology, Faculty of Medicine, Prince of Songkla University, Hat Yai, Songkhla 90110, Thailand.

[2]Department of Orthopaedic Surgery and Physical Medicine, Faculty of Medicine, Prince of Songkla University, Hat Yai, Songkhla 90110, Thailand.

Received 25 May 2024 ● Revised 27 June 2024 ● Accepted 9 July 2024 ● Published online 8 January 2025

Abstract:

Objective: Plain radiographs are vital for initial evaluations of bone tumors. However, multiplanar imaging; like magnetic resonance imaging (MRI), is often necessary for inconclusive cases. Hence, we aimed to determine the diagnostic value of MRI in evaluating bone tumor matrix and analyzing MRI characteristics of the matrix.

Material and Methods: This study reviewed 245 MRI and plain radiographs of pathologically confirmed bone tumors; including 123 mineralized and 122 non-mineralized bone tumors. A radiologist having 16 years of experience assessed tumor matrix characteristics, including border, signal intensity on T1-weighted (T1W), T2-weighted (T2W), and gradient-echo images, along with enhancement patterns. Sensitivity, specificity, and a 95% confidence interval were used to present diagnostic values.

Results: MRI demonstrated a sensitivity and specificity of 78.1% and 87.7% in differentiating mineralized from non-mineralized matrices, compared to 75.6% and 92.6% for plain radiographs. Both modalities showed high sensitivity and specificity in evaluating osteoid and chondroid matrices (MRI: 80.3%/84.0%, 94.5%/96.8%; radiographs: 80.3%/72.0%, 95.1%/96.4% specificity). High specificity was noted in evaluating fibrous matrices (97.4%/99.6%) but with low sensitivity (23.5%/11.8%). MRI outperformed radiographs in subcategorizing fat, soft tissue, and cystic tumors. The chondroid matrix exhibited distinct characteristics on MRI (well-defined lobulated border with high/intermediate T2W and lobulated/peripheral enhancement), while osteoid and fibrous matrices showed similar features, except in T1W signal intensity. Non-mineralized tumors displayed varied characteristics.

Contact: Pramot Tanutit, M.D.
Department of Radiology, Faculty of Medicine, Prince of Songkla University, Songkhla 90110, Thailand.
E-mail: ptanutit@yahoo.com

J Health Sci Med Res
doi: 10.31584/jhsmr.20251137
www.jhsmr.org

Conclusion: While plain radiographs are essential for initial bone tumor assessment, especially for mineralization, MRI is superior in evaluating tumor matrices and non-mineralized tissues in providing detailed characterization for staging and treatment planning.

Keywords: bone tumor, bone tumor matrix, magnetic resonance imaging, mineralization

Introduction

Malignant bone tumors are one of the major causes of death globally; especially among children and adolescents. It has been reported that 3,970 bone tumor patients were diagnosed annually, and approximately 2,140 cases resulted in fatalities within the USA in 2023[1]. While the incidence of bone tumors is not as high as that of other types of tumors, this disease still necessitates precise diagnosis for specific treatment.

The diagnosis of bone tumors requires both clinical information and diagnostic imaging. Plain radiographs play an initial role in disease evaluation, while radiographic images provide information regarding tumor location and aggressiveness; including details about margins, periosteal reactions, cortical changes and the presence of soft tissue components[2-4]. This imaging modality also offers insights into tumor mineralization, aiding radiologists in predicting tumor types[2]. However, in cases of inconclusive bone tumors, further investigation is necessary.

Advanced imaging; including computed tomography (CT) and magnetic resonance imaging (MRI), play important roles in further bone tumor evaluation. The use of advanced imaging in the assessment of bone tumors has increased, particularly MRI, because the modality provides excellent soft tissue contrast and can guide differentiation between aggressive and nonaggressive bone lesions[5]. However, the use of MRI in the evaluation of bone tumor mineralization in routine practice remains unclear. Based on our literature review, no studies have examined the diagnostic value of bone tumor mineralization and MRI characteristics in evaluating bone tumor matrix. This identified gap in the literature prompted us to conduct this present study.

This retrospective study aimed to determine the diagnostic value of MRI in evaluating bone tumor matrix, using pathology-proven cases as the reference. Additionally, the characteristics of bone tumor matrices identified by MRI were assessed.

Material and Methods

This retrospective study was conducted at a university tertiary hospital in southern Thailand. We reviewed the MRI and plain radiographs of patients having pathologically proven bone tumors at any site from January 1st, 2006 to January 1st, 2019. Eligible criteria included : (1) patients with pathologically proven bone tumors of any age group; (2) patients having undergone plain radiographs and MRI at the tumor site before receiving specific treatment; and (3) patients for whom the MRI sequence included T1-weighted images (T1W), T2-weighted images (T2W), and T1W contrast-enhanced fat-suppressed images. Patients with poor-quality MRI or plain radiographs were excluded. This study was approved by the Ethics Committee of the study hospital (REC 60-427-07-4).

The MRI and plain radiographs of the bone tumors were selected and separately reviewed by a musculoskeletal radiologist with 16 years of experience (PT). The MRI and radiographs of each patient were reviewed with a one-month gap between the modalities. The reviewing radiologist was blinded to the patient's clinical information, tumor diagnosis, and tumor matrix. We used the pathological

results as a reference standard to categorize bone tumors into osteoid, chondroid, fibrous, and non-mineralized matrix groups, including fat, cyst, and non-mineralized soft tissue. Mineralized bone tumors were classified as those with matrices that could be detected on plain radiographs, such as osteoid, chondroid, and fibrous subgroups. The rest were classified as non-mineralized subgroups, with matrices that could not be detected on plain radiographs.

The MRI characteristics of the bone tumor matrix were evaluated. The border of the bone tumor matrix was classified as well-defined lobulated, well-defined smooth, and ill-defined/patchy patterns; as identified on T2W images (Figure 1). Signal intensity (SI) of the matrix on T1W and T2W images was classified as: low, intermediate, high, and mixed SI as compared to muscle SI. The enhancement of the tumor matrix was classified as presence and absence. The pattern of matrix enhancement was classified as homogeneous or patchy enhancement, heterogeneous or lobulated enhancement, septal/peripheral enhancement, and combined patterns of enhancement. Susceptibility artifact on gradient-recalled echo images (GRE) was also classified as presence and absence. Finally, the reviewer categorized the final decision for the tumor matrix into osteoid, chondroid, fibrous, and non-mineralized groups; including fat, cyst, and non-mineralized soft tissue. Tumors without identified matrices were categorized into the non-mineralized group. Tumors with fatty foci were classified into the fat group. Purely cystic tumors were classified into the cystic group. The remaining tumors; including pure soft tissue and soft tissue with cystic components, were classified as the non-mineralized soft tissue group.

The plain radiographs of the bone tumors were also evaluated. The tumor matrix in plain radiographs was classified based on presence or absence and then categorized into osteoid, chondroid, fibrous, and non-mineralized groups.

The diagnostic value was calculated using R software version 3.5.1 and MedCalc statistical software to determine diagnostic indices; including sensitivity, specificity, 95% confidence interval (95% CI), positive predictive value (PPV), negative predictive value (NPV), positive likelihood ratio (PLR) and negative likelihood ratio (NLR). Descriptive statistics were expressed as a percentage and median with interquartile range (IQR). The Mann–Whitney U-test was used to estimate differences in continuous data between the groups of bone tumor matrix. Fisher's exact test was used for categorical data. A p-value of less than 0.05 was considered statistically significant.

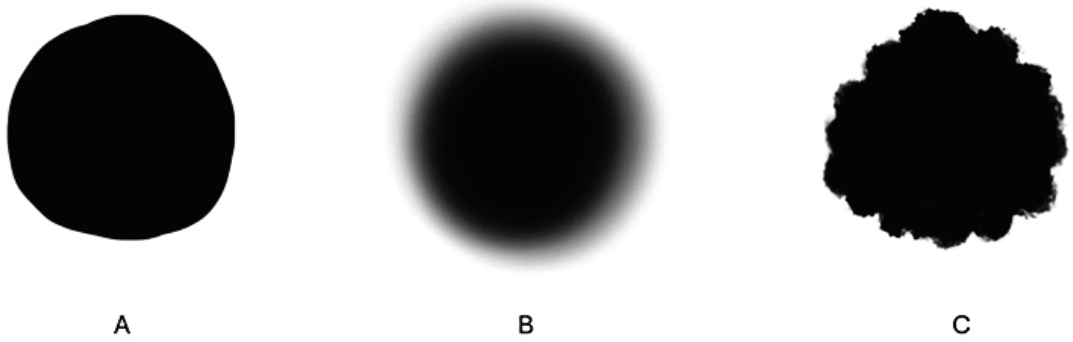

Figure 1 Borders of the bone tumor matrix classified as: (A) well-defined smooth, (B) ill-defined/patchy, and (C) well-defined lobulated patterns

Results

Demographic characteristics

We retrospectively reviewed 245 patients with pathologically proven bone tumors. Table 1 presents the demographic characteristics of patients with pathologically proven bone tumors, stratified by tumor mineralization. The percentages of bone tumors with mineralized and non-mineralized matrices were approximately 51.2% and 49.8%, respectively. The osteoid matrix was the most common subtype in the mineralized group (81 patients; 33.1%). Chondroid and fibrous-containing tumors were 10.2% and 6.9%, respectively. In the non-mineralized bone tumors group, tumors with a soft tissue component represented the highest percentage (36.7%) compared to tumors with cysts and fat (12.7% and 0.4%, respectively). The median age of patients in the mineralized and non-mineralized tumor groups was 17 and 43.5 years, respectively (p-value<0.001). Patients with an osteoid matrix had the lowest median age (15 years), whereas patients with soft tissue tumors without a mineralized matrix had the highest median age (50 years). There were no statistically significant differences in the gender distribution between the mineralized and non-mineralized groups. Most bone tumors were located in long bones: constituting approximately 83.7% of the total. Mineralized tumors were significantly more prevalent in long bones compared to non-mineralized tumors (110 patients; 89.4% and 95 patients; 77.9%, respectively: p-value=0.023).

A total of 67 patients (27.3%) were diagnosed with osteosarcoma, followed by metastasis in 19.2% (47 patients), giant cell tumor in 10.2% (25 patients), and Ewing sarcoma in 7.3% (18 patients). The remaining diagnoses (36.0%) included: malignant fibrous histiocytoma, osteochondroma, chondrosarcoma, multiple myeloma, plasmacytoma, chordoma, lymphoma, leukemia, aneurysmal bone cyst, simple bone cyst; fibrous dysplasia, osteoblastoma, osteoid osteoma, chondromyxoid fibroma, enchondroma; malignant hemangiopericytoma, spindle cell sarcoma, intraosseous lipoma, embryonal rhabdomyosarcoma, crystal-storing histiocytosis and Langerhans cell histiocytosis.

Diagnostic value of MRIs and radiographs in evaluation of bone tumor matrix

Table 2 displays the overall diagnostic value of MRI in differentiating between pathologically proven mineralized and non-mineralized tumor matrices. The sensitivity of MRI and plain radiographs in evaluating bone tumor matrices was high for both (78.1%, 95% CI=69.69-85.01 and 75.6%, 95% CI=67.05-82.90, respectively). However, the specificity of plain radiographs in evaluating bone tumor matrices was higher than that of MRI (92.6; 95% CI=86.46-96.57 and 87.7, 95% CI=80.53-92.95, respectively). Additionally, the PPV and PLR of plain radiographs were higher than those of MRI, while the NPV and NLR were almost similar.

The sensitivity and specificity of MRI and plain radiographs in the evaluation of each subtype of bone tumor matrix are presented in Table 3. MRI interpretation of the mineralized matrix demonstrated high sensitivity and specificity in osteoid and chondroid tumors: a sensitivity of 80.3% (95% CI=69.91-88.27) and specificity of 94.5% (95% CI=89.84-97.46) for osteoid; and a sensitivity of 84.0% (95% CI=63.92-95.46) and specificity of 96.8% (95% CI=93.55-98.71) for chondroid. MRI also exhibited excellent sensitivity and specificity in fat-containing tumors and tumors with non-mineralized soft tissue components. However, the sensitivity of MRI in the evaluation of fibrous matrix and cyst was low (23.5%, 95% CI=6.81-49.90 and 32.3%, 95% CI=16.68-51.37, respectively), while the specificity was high (97.4%, 95% CI=94.36-99.03 and 98.1%, 95% CI=95.28-99.49, respectively).

Similarly, plain radiographs demonstrated high sensitivity and specificity in the evaluation of osteoid and chondroid matrices: a sensitivity of 80.3% (95% CI = 69.91-88.27) and specificity of 95.1% (95% CI=90.61-97.87) for

Table 1 Demographic characteristics of patients with bone tumor matrices

Variables	Overall	Mineralized tumors				Non-mineralized tumors				p-value
	N=245	Total	Osteoid	Chondroid	Fibrous	Total	Fat	Soft tissue	Cystic	
	n(%)	123 (51.2)	81 (33.1)	25 (10.2)	17 (6.9)	122 (49.8)	1 (0.4)	90 (36.7)	31 (12.7)	
Age: median (IQR)	28 (14,51)	17 (13,32)	15 (12,21)	27 (17,47)	44 (23,52)	43.5 (26,58.8)	23 (NA)	50 (30,61)	32 (21.5,37.5)	<0.001
Gender: male n(%)	129 (52.7)	60 (48.8)	43 (71.7)	9 (15.0)	8 (13.3)	69 (56.6)	0 (0.0)	51 (73.9)	18 (26.1)	0.275
Location: long bone n(%)	205 (83.7)	110 (89.4)	75 (68.2)	19 (17.3)	16 (14.5)	95 (77.9)	1 (1.0)	65 (68.4)	29 (30.6)	0.023

IQR=interquartile range, NA=not applicable

Table 2 Diagnostic values of MRI and radiographs in differentiating pathologically proven mineralized tumor matrices from non-mineralized bone tumors

Modality	Sensitivity	Specificity	PPV	NPV	PLR	NLR
	% (95% CI)					
MRI	78.1 (69.69-85.01)	87.7 (80.53-92.95)	86.5 (78.69-92.23)	79.9 (72.05-86.28)	6.4 (3.91-10.29)	0.3 (0.18-0.35)
Radiograph	75.6 (67.05-82.90)	92.6 (86.46-96.57)	91.2 (83.91-95.89)	79.0 (71.43-85.38)	10.3 (5.42-19.37)	0.3 (0.19-0.36)

PPV=Positive predictive value, NPV=Negative predictive value, PLR=Positive likelihood ratio, NLR=Negative likelihood ratio, 95% CI=95% confidence interval, MRI=magnetic resonance imaging

osteoid; a sensitivity of 72.0% (95% CI=50.61-87.93) and specificity of 96.4% (95% CI=92.96-98.42) for chondroid. In the case of the fibrous matrix, the sensitivity was low, while the specificity was high (11.8%, 95% CI=1.46-36.44, and 99.6%, 95% CI=97.58-99.99, respectively). Plain radiographs also exhibited high sensitivity and specificity for bone tumors without a mineralized matrix.

MRI characteristics of bone tumor matrix

The MRI characteristics of bone tumors with mineralized and non-mineralized matrices are presented in Table 4. In mineralized tumor matrices, the percentage of ill-defined/patchy borders was higher in the osteoid and fibrous matrix groups (95.1%; 77 patients and 94.0%; 16 patients) compared to the chondroid group (8.0%; 2 patients). In contrast, well-defined lobulated and well-defined smooth borders were more prevalent in the chondroid group: accounting for about 72.0% (18 patients) and 20.0% (5 patients), respectively. Approximately half of the osteoid matrix exhibited low SI on T1W, while more than half of the chondroid and fibrous matrices showed intermediate SI (60.0% and 70.6%, respectively). On

Table 3 Sensitivity and specificity of MRI and radiographs in the evaluation of bone tumor matrices

Tumor matrix	MRI		Radiograph	
	Sensitivity (95% CI)	Specificity (95% CI)	Sensitivity (95% CI)	Specificity (95% CI)
Osteoid matrix	80.3 (69.91–88.27)	94.5 (89.84–97.46)	80.3 (69.91–88.27)	95.1 (90.61–97.87)
Chondroid matrix	84.0 (63.92–95.46)	96.8 (93.55–98.71)	72.0 (50.61–87.93)	96.4 (92.96–98.42)
Fibrous matrix	23.5 (6.81–49.90)	97.4 (94.36–99.03)	11.8 (1.46–36.44)	99.6 (97.58–99.99)
Non-mineralized			92.6 (86.46–96.57)	75.6 (67.05–82.90)
Fat	100.0 (2.50–100.00)	100.0 (98.50–100.00)		
Soft tissue	90.0 (81.86–95.32)	73.6 (65.87–80.30)		
Cystic component	32.3 (16.68–51.37)	98.1 (95.28–99.49)		

95% CI=95% confidence interval, MRI=magnetic resonance imaging

Table 4 MRI characteristics of pathologically proven groups of bone tumors

MRI characteristic	Mineralized tumors on radiographs			Non-mineralized tumors on radiographs		
	Osteoid N=81 n (%)	Chondroid N=25 n (%)	Fibrous N=17 n (%)	Fat N=1 n (%)	Soft tissue N=90 n (%)	Cystic N=31 n (%)
Border						
Well-defined lobulated	3 (3.7)	18 (72.0)	0 (0.0)	0 (0.0)	10 (11.1)	16 (51.6)
Well-defined smooth	1 (1.2)	5 (20.0)	1 (5.9)	1 (100)	0 (0.0)	0 (0.0)
Ill-defined/Patchy	77 (95.1)	2 (8.0)	16 (94.1)	0 (0.0)	80 (88.9)	15 (48.4)
T1W						
Low	41 (50.6)	3 (12.0)	3 (17.6)	0 (0.0)	10 (11.1)	0 (0.0)
Intermediate	14 (17.3)	15 (60.0)	12 (70.6)	0 (0.0)	53 (58.9)	13 (41.9)
High	1 (1.2)	0 (0.0)	0 (0.0)	1 (100)	0 (0.0)	0 (0.0)
Mixed	25 (30.9)	7 (28.0)	2 (11.8)	0 (0.0)	27 (30)	18 (58.1)
T2W						
Low	47 (58.0)	4 (16)	4 (23.5)	0 (0.0)	4 (4.4)	2 (6.5)
Intermediate	1 (1.2)	4 (16)	5 (29.4)	0 (0.0)	34 (37.8)	2 (6.5)
High	1 (1.2)	8 (32)	2 (11.8)	1 (100)	12 (13.3)	4 (12.9)
Mixed	32 (39.5)	9 (36)	6 (35.3)	0 (0.0)	40 (44.4)	23 (74.2)
Enhancement: present	39 (48.1)	25 (100)	13 (76.5)	1 (100)	88 (97.8)	31 (100)
Pattern of enhancement						
Homogeneous/patchy	14 (35.9)	2 (8.0)	6 (35.3)	0 (0.0)	47 (52.2)	7 (22.6)
Heterogeneous/lobulated	15 (38.5)	10 (40.0)	4 (23.5)	0 (0.0)	29 (32.2)	11 (35.5)
Septal/peripheral	9 (23)	10 (40.0)	1 (5.9)	1 (100)	7 (7.8)	10 (32.3)
Combined pattern	1 (2.6)	3 (12.0)	2 (11.8)	0 (0.0)	5 (5.6)	3 (9.7)
Susceptibility artifact	59/60 (98.3)	12/20 (60.0)	4/9 (44.4)	0/1 (0.0)	17/31 (54.8)	17/22 (77.3)

T1W=T1-weighted image, T2W=T2-weighted image, MRI=magnetic resonance imaging

T2W, the majority of the osteoid matrix displayed low and mixed SI; approximately 58.0% and 39.5%, respectively. About half of the chondroid matrix exhibited intermediate and high SI on T2W (48%), with approximately one-third showing mixed SI. In the case of the fibrous matrix, the signal intensity on T2W varied, with the most common pattern being mixed SI (35.3%). All chondroid matrices showed enhancement, while only 48.1% of osteoid matrices and 76.5% of fibrous matrices showed enhancement. In terms of the enhancement pattern, approximately one-third of the osteoid matrix exhibited homogeneous/patchy enhancement (35.9%; 14 patients), while heterogeneous/lobulated enhancement was observed in 38.5% (15 patients). However, the majority of the chondroid matrix displayed heterogeneous/lobulated enhancement and septal/peripheral enhancement, approximately 40.0% for each. For the fibrous matrix, most showed homogeneous/patchy enhancement (35.3%), followed by heterogeneous/lobulated enhancement (23.5%). The susceptibility artifact in GRE images was approximately 98.3%, 60.0%, and 44.4% for the osteoid, chondroid, and fibrous matrices, respectively.

For non-mineralized bone tumors, there was one case of a fat-containing tumor, showing a well-defined smooth border with high SI on T1W, high SI on T2W, and peripheral enhancement. Regarding the tumors with a non-mineralized soft tissue component, 88.9% of this group showed an ill-defined/patchy border (80 patients), while tumors with a cystic component showed well-defined lobulated and ill-defined/patchy features; each accounting for about 50.0%. The majority of tumors with a soft tissue component and those with cysts showed intermediate SI and mixed SI on T1W. On T2W, mixed SI was the most common pattern in tumors with a soft tissue component (44.4%), followed by intermediate SI (37.8%), while three-quarters of the tumors with cysts showed mixed SI on T2W (74.2%). Overall, nearly all tumors with a non-mineralized matrix exhibited enhancement. The majority pattern of enhancement in the tumors with a soft tissue component was homogeneous/patchy enhancement (52.2%; 47 patients), followed by heterogeneous/lobulated enhancement (32.2%; 29 patients). About two-thirds of the tumors with cysts showed heterogeneous/lobulated patterns and septal/peripheral patterns (35.5% and 32.3%, respectively).

Discussion

Our study aimed to evaluate the diagnostic value of MRI in distinguishing mineralized bone tumors from non-mineralized tumors, utilizing pathological results as the reference standard. It was found that both MRI and plain radiographs exhibited high sensitivity in evaluating bone tumor matrices, with MRI demonstrating greater sensitivity than plain radiographs. However, plain radiographs demonstrated higher specificity. This indicates that while MRI is more sensitive in detecting the presence of tumor matrices, plain radiographs are more specific in accurately categorizing them.

When comparing subtypes of mineralized bone tumor matrices, high sensitivity and specificity of MRI in the interpretation of osteoid and chondroid tumors were found. This suggests that MRI is a reliable tool for diagnosing these types of bone tumors. Plain radiographs also demonstrated high sensitivity and specificity in evaluating osteoid and chondroid matrices; nearly paralleling the MRI's performance. This finding is particularly relevant in clinical settings with limited MRI availability, as it suggests that plain radiographs can be a valuable diagnostic tool for the initial evaluation of osteoid and chondroid tumors. Both MRI and plain radiographs provided low sensitivity and high specificity for fibrous matrix in our study. This suggests that while MRI and plain radiographs are highly specific in ruling out fibrous-containing tumors, they may not be as effective in correctly identifying all cases. However, MRI is superior to plain radiographs in categorizing non-

mineralized bone tumors, as it can categorize the tumors into fat, soft tissue, and cyst subgroups. Additionally, MRI has been known to be an advantageous modality in the evaluation of the soft tissue component of bone tumors[5–7]. In both fat- and soft tissue-containing tumors, it was found that MRI provided high sensitivity and specificity. However, MRI exhibited low sensitivity in the evaluation of tumors with a cystic component. This may be because fat and soft tissue components are clearly evaluated using MRI. Also, when there is a combined portion of cystic, blood, necrotic, and soft tissue components in each case, indicating uncertainty for the radiologist to subcategorize the tumors into these groups.

It was found that the MRI characteristics of mineralized tumor matrices revealed variations in border definitions and SI across different subtypes. Osteoid and fibrous matrices share similar characteristics, including borders and patterns of enhancement. Most osteoid and fibrous matrices showed an ill-defined/patchy border, with homogeneous/patchy or homogeneous/lobulated enhancement (Figure 2.1 and 2.2). However, these two matrices showed differences in SI. While most of the osteoid matrix exhibited low or mixed SI on T1W and T2W, the fibrous matrix showed intermediate SI on T1W and variable SI on T2W. Studies conducted on these subtypes of bone tumors have revealed findings similar to ours. The osteoid matrix showed low SI on both T1W and T2W images, while the fibrous component typically displays intermediate SI on T1W in addition to variable low signal intensity on T2W[8–12]. The low signal intensity of osteoid tumors on T1W and T2W, similar to the bony cortex, results from a reduced number of mobile protons available to generate the MR signal[13]. However, the chondroid matrix revealed unique characteristics. In our study, most of the chondrogenic tumors exhibited a well-defined lobulated/smooth border, intermediate SI on T1W, variable SI on T2W, and lobulated or peripheral/septal enhancement (Figure 2.3). All of the chondroid matrices exhibited enhancement. Several studies have been conducted on the characteristics of chondrogenic tumors, and their results are similar to our findings[8,14–17]. The variable T2W component of the chondroid matrix could result from a high T2W component due to the high water content of hyaline cartilage and a low T2W component arising from immature chondroid matrix, calcifications, or chronic hemorrhage[6,18,19]. Susceptibility artifacts on GRE images varied among different matrices, possibly indicating distinct mineralization properties. However, almost all cases of the osteoid matrix exhibited susceptibility artifacts on GRE images that differed from those in chondroid and fibrous matrices. This can be explained by the fact that susceptibility artifacts are caused by paramagnetic substances, creating blooming foci on gradient techniques[20,21]. The mineralized osteoid matrix is predominantly composed of calcification/ossification components, resulting in susceptibility artifacts in most cases. However, the hemosiderin substance from blood components also exhibits susceptibility artifacts[20,21]. Therefore, chondroid or fibrous matrices containing calcifications or blood components also showed susceptibility artifacts on GRE.

For non-mineralized matrices, we found the prevalence of tumors with a soft tissue component and the distinctive features of those with cystic components The majority of these tumors exhibited intermediate and mixed SI on T1W and T2W, emphasizing the complexity of the internal composition (Figure 3.1 and 3.2). Enhancement patterns in these tumors varied, with a predominant homogeneous/patchy pattern in those with a soft tissue component and heterogeneous/lobulated patterns in cystic tumors. Cystic-containing tumors typically exhibit high SI on T2W and variable SI on T1W, accompanied by septal or peripheral enhancement[22]. The variation in SI is attributed to the diverse internal components of these tumors[6]. Similarly, soft tissue components without mineralization, characterized by a variety of cell types, also display variable signal intensity

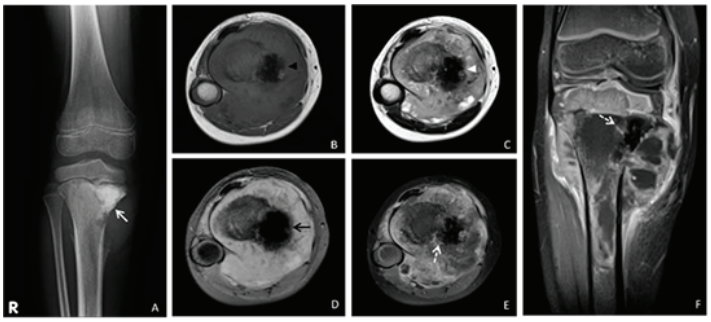

Figure 2.1

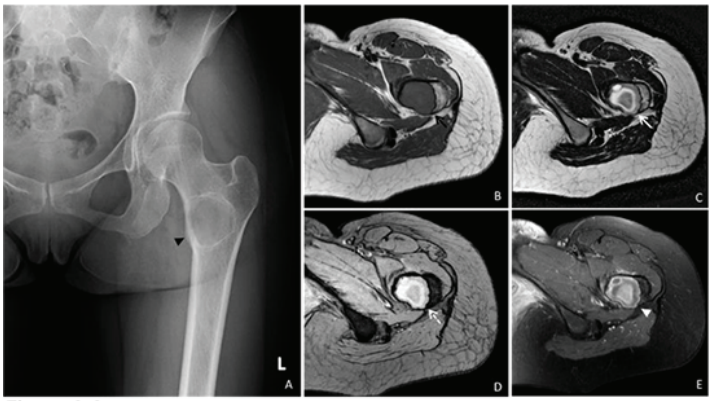

Figure 2.2

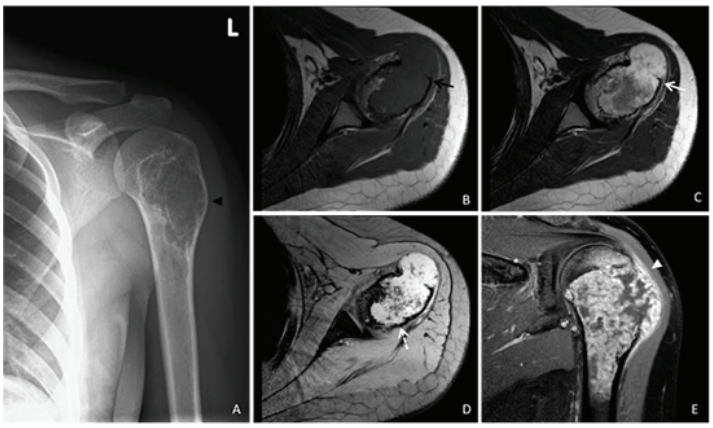

Figure 2.3

Figure 2 Figure 2.1 A 9–year–old boy with osteosarcoma at the right proximal tibia. (A) The matrix on a plain radiograph shows an ivory–like matrix representing the osteoid matrix (white arrow). (B) Axial T1W (C) and axial T2W MR images of the tibia show an ill–defined/patchy border of low signal intensity of the osteoid matrix on both T1W (black arrowhead) and T2W images (white arrowhead). (D) The susceptibility artifact on the GRE image is seen (black arrow). Some areas of heterogeneous enhancement are shown on (E) axial and (F) coronal T1W fat–saturated MR images with gadolinium enhancement (dotted white arrow); Figure 2.2 A 25–year–old woman with fibrous dysplasia at the left proximal femur. (A) The plain radiograph shows a well–defined geographic osteolytic lesion, with a ground glass appearance at the left proximal femoral metaphysis; compatible with

fibrous dysplasia with a fibrous matrix (black arrowhead). It shows a well-defined smooth border of the fibrous matrix, with homogeneously intermediate signal intensity on (B) axial T1W image (black arrow), mixed signal intensity on (C) axial T2W image (white arrow), and no susceptibility artifact on (D) GRE image (dotted white arrow). (E) Axial T1W fat-saturated MR image with gadolinium enhancement shows lobulated enhancement of the fibrous matrix (white arrowhead); Figure 2.3 A 21-year-old woman with chondrosarcoma at the left humerus. (A) The plain radiograph shows an ill-defined geographic osteolytic lesion at the metaphysis of the left proximal humerus, with an internal ring-and-arc chondroid matrix (black arrowhead). The chondroid matrix shows a well-defined lobulated border, with intermediate signal intensity on (B) axial T1W image (black arrow) and high signal intensity on (C) axial T2W image (white arrow). (D) Multiple small foci of susceptibility artifacts on the GRE image are seen (dotted white arrow). (E) Coronal T1W fat-saturated MR image with gadolinium enhancement shows lobulated enhancement of the chondroid matrix (white arrowhead)

and enhancement patterns, which are dependent on their internal composition[8,18]. There was only one case of a tumor containing fat in our study, which exhibited typical findings of an intraosseous lipoma (Figure 3.3). This led to superior sensitivity and specificity in identifying fat-containing tumors.

We found that the median age of patients with a mineralized tumor matrix was statistically significantly lower than that of the non-mineralized tumor group. Additionally, the prevalence of long bone locations in mineralized tumors was significantly higher compared to the non-mineralized group. This can be explained by the high prevalence of osteosarcoma in our study (67 patients; 27.3%), which is part of the osteoid matrix subgroup and predominantly affects the adolescent and young adult population[13,23,24]. Metastasis was the second most common tumor type in our study (47 patients; 19.2%), along with a certain percentage of multiple myeloma and plasmacytoma cases, all of which belong to the non-mineralized tumor group. These tumors are more prevalent in older age groups and tend to occur in marrow-rich locations; particularly in flat bones[25-27]. These factors elucidate the differences between the mineralized and non-mineralized groups in our study.

Evaluation of the bone tumor matrix is crucial, as it aids clinicians in establishing a definitive diagnosis and determining appropriate treatment strategies[28]. Plain radiography is a primary tool for investigating bone tumors due to its ability to reveal tumor aggressiveness and offer detailed pathological guidance[2,18]. However, the development of MRI techniques has expanded the role of MRI in the evaluation of bone tumors; including the assessment of the tumor matrix[4-7,18,29-32]. The significant increase in the utilization of cross-sectional imaging modalities for bone tumor evaluation is a notable trend.

Our study had certain limitations. Firstly, being a retrospective study, it faced constraints with limited patient information, a non-standardized MRI protocol, and a small sample size. Secondly, being a single-center study, it may not represent the generalizability of the study population. However, we adhered to an eligible protocol to include all patients. Lastly, the MRIs in our study were reviewed by a single, experienced radiologist and this may have limited our ability to evaluate inter-reader reliability using the Kappa value. Future studies involving multiple radiologists are recommended to better assess inter-reader reliability in the interpretation of tumor matrix evaluation on MRIs.

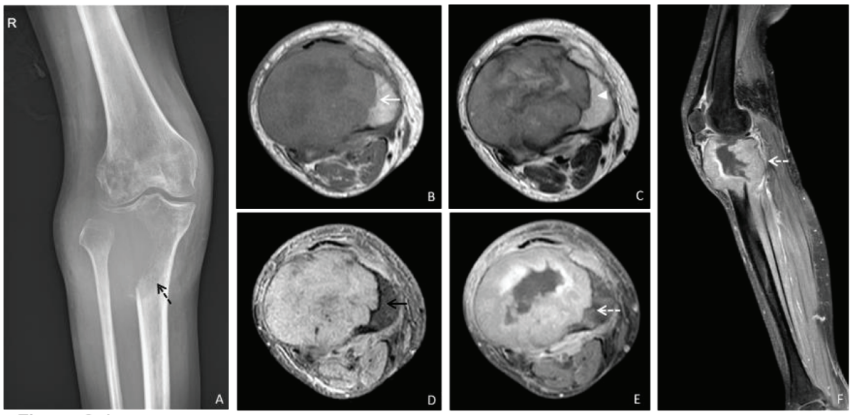

Figure 3.1

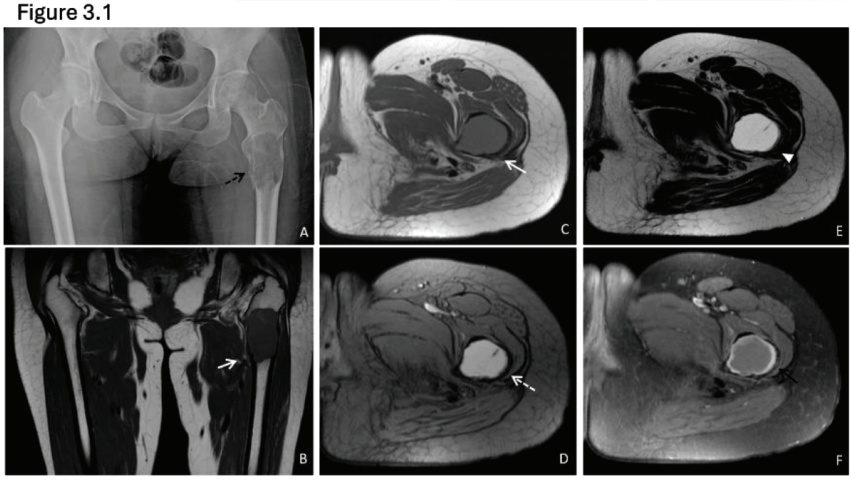

Figure 3.2

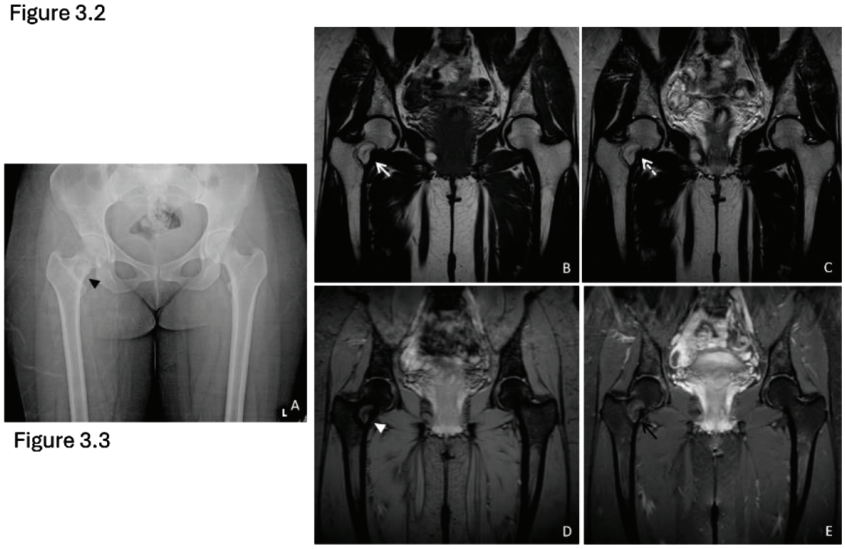

Figure 3.3

Figure 3 Figure 3.1 A 36-year-old woman with a giant cell tumor at the right proximal tibia, representing a non-mineralized soft tissue tumor. (A) Plain radiograph shows an ill-defined geographic osteolytic lesion at the lateral aspect of the right tibial epi-metaphysis without visualized mineralized matrix (dotted black arrow). The tumor shows

a well-defined lobulated border, with intermediate signal intensity on (B) axial T1W image (white arrow) and mixed signal intensity on (C) axial T2W image (white arrowhead), without susceptibility artifact on (D) GRE image (black arrow). (E) Axial and (F) sagittal T1W fat-saturated MR images with gadolinium enhancement show homogeneous patchy enhancement, with a central non-enhanced portion (dotted white arrow); Figure 3.2 A 24-year-old woman with a simple bone cyst in the left proximal femur. (A) Plain radiograph of the simple bone cyst reveals a well-defined geographic osteolytic lesion, containg a sclerotic margin (dotted black arrow), with no internal mineralized matrix visible. A pathologic fracture at the medial aspect of the cyst is noted. (B) Coronal and (C) axial T1W images show the cyst having a well-defined lobulated border and intermediate signal intensity (white arrow). (D) No susceptibility artifact is seen on the GRE image (dotted white arrow). The cyst shows high signal intensity on (E) axial T2W image (white arrowhead). (F) Axial T1W fat-saturated MR image with gadolinium enhancement shows peripheral enhancement of the simple bone cyst (black arrow); Figure 3.3 A 23-year-old woman with intraosseous lipoma at the right proximal femur. (A) A well-defined geographic osteolytic lesion, with a sclerotic margin at the right femoral neck is found; without demonstrable mineralized matrix. The lipoma shows a well-defined smooth border having high signal intensity on (B) coronal T1W (white arrow) and (C) coronal T2W images (dotted white arrow), without susceptibility artifact on (D) GRE image (white arrowhead). (E) Coronal T1W fat-saturated MR image with gadolinium enhancement shows peripheral enhancement of the lipoma (black arrow).

Conclusion

In conclusion, our findings highlight the complementary roles of MRI and plain radiographs in evaluating bone tumors. While plain radiographs are essential as an initial assessment tool for bone tumors and their mineralization, MRI offers high diagnostic performance in evaluating both tumor matrices and non-mineralized soft tissue components. Furthermore, MRI can serve as an alternative imaging modality in the evaluation of bone tumors, as it provides detailed tumor characterization and staging and aids in treatment planning. However, further research is required to assess the significant differences between matrix subtypes as observed on MRI.

Acknowledgement

We are thankful to Jirawan Jayuphan, Department of Epidemiology, Faculty of Medicine, Prince of Songkla University, for population calculation and data analysis.

Conflict of interest

The authors declare that there is no conflicts of interest.

References

1. Siegel RL, Miller KD, Wagle NS, Jemal A. Cancer statistics, 2023. CA Cancer J Clin 2023;73:17–48.
2. Miller TT. Bone tumors and tumorlike conditions: analysis with conventional radiography. Radiology 2008;246:662–74.
3. Woertler K. Benign bone tumors and tumor-like lesions: value of cross-sectional imaging. Eur Radiol 2003;13:1820–35.
4. Sundaram M, McLeod RA. MR imaging of tumor and tumorlike lesions of bone and soft tissue. Am J Roentgenol 1990;155:817–24.
5. Tanutit P, Pakdee W, Laohawiriyakamol T, Iamthanaporn K. Magnetic resonance imaging in differentiating between aggressive and non-aggressive bone tumors. Acta Radiol 2023;64:625–37.
6. Nascimento D, Suchard G, Hatem M, de Abreu A. The role of magnetic resonance imaging in the evaluation of bone tumours and tumour-like lesions. Insights Imaging 2014;5:419–40.

7. Griffiths HJ, Galloway HR, Thompson RC, Suh J, Nelson T. The use of MRI in the diagnosis of benign and malignant bone and soft tissue tumours. Australas Radiol 1993;37:35–9.
8. Golfieri R, Baddeley H, Pringle JS, Leung AWL, Greco A, Souhami R, et al. Primary bone tumors: MR morphologic appearance correlated with pathologic examinations. Acta Radiol 1991;32:290–8.
9. Murphey D. The many faces of osteosarcoma. Radiographics 1997;17:1205–31.
10. Finkelstein D, Foremny G, Singer A, Clifford P, Pretell–Mazzini J, Kerr D, et al. Differential diagnosis of T2 hypointense masses in musculoskeletal MRI. Skeletal Radiol 2021;50:1981–94.
11. Kato H, Kawaguchi M, Miyase R, Iwashima K, Nagano A, Matsuo M. Comparison of MRI Findings among Osteofibrous Dysplasia, Fibrous Dysplasia, and NonOssifying Fibroma of the Long Bone. Indian J Radiol Imaging 2023;33:150–6.
12. Jelinek JS, Murphey MD, Kransdorf MJ, Shmookler BM, Malawer MM, Hur RC. Parosteal osteosarcoma: value of MR imaging and CT in the prediction of histologic grade. Radiology 1996;201:837–42.
13. Yarmish G, Klein MJ, Landa J, Lefkowitz RA, Hwang S. Imaging characteristics of primary osteosarcoma: nonconventional subtypes. Radiographics 2010;30:1653–72.
14. Geirnaerdt MJ, Bloem JL, Eulderink F, Hogendoorn PC, Taminiau AH. Cartilaginous tumors: correlation of gadolinium–enhanced MR imaging and histopathologic findings. Radiology 1993;186:813–7.
15. Geirnaerdt MJA, Hogendoorn PCW, Bloem JL, Taminiau AHM, van der Woude H. Cartilaginous Tumors: Fast Contrast–enhanced MR Imaging. Radiology 2000;214:539–46.
16. Murphey MD, Flemming DJ, Boyea SR, Bojescul JA, Sweet DE, Temple HT. Enchondroma versus chondrosarcoma in the appendicular skeleton: differentiating features. Radiogr Rev Publ Radiol Soc N Am Inc 1998;18:1213–37.
17. Littrell LA, Wenger DE, Wold LE, Bertoni F, Unni KK. Radiographic, CT, and MR Imaging Features of Dedifferentiated Chondrosarcomas: A Retrospective Review of 174 De Novo Cases. Radiographics 2004;24:1397–09.
18. Hwang S, Panicek DM. The Evolution of Musculoskeletal Tumor Imaging. Radiol Clin North Am 2009;47:435–53.
19. Kim JH, Lee SK. Classification of chondrosarcoma: from characteristic to challenging imaging findings. Cancers 2023;15:1703.
20. Bitar R, Leung G, Perng R, Tadros S, Moody AR. MR pulse sequences: what every radiologist wants to know but is afraid to ask. Radiographics 2006;26:513–37.
21. Tang MY, Chen TW, Zhang XM, Huang XH. GRE T2*–weighted mri: principles and clinical applications. BioMed Res Int 2014;2014:312142.
22. Fayad LM, Jacobs MA, Wang X, Carrino JA, Bluemke DA. Musculoskeletal tumors: how to use anatomic, functional, and metabolic MR techniques. Radiology 2012;265:340–56.
23. Udomruk S, Phanphaisarn A, Kanthawang T, Sangphukieo A, Sutthitthasakul S, Tongjai S, et al. Characterization of cell–free dna size distribution in osteosarcoma patients. Clin Cancer Res 2023;29:2085–94.
24. Kanthawang T, Wudhikulprapan W, Phinyo P, Settakorn J, Pruksakorn D, Link TM, et al. Can conventional magnetic resonance imaging at presentation predict chemoresistance in osteosarcoma? Br J Radiol 2024;97:451–61.
25. Hu Z, Yang S, Xu Z, Zhang X, Wang H, Fan G, et al. Prevalence and risk factors of bone metastasis and the development of bone metastatic prognostic classification system: a pan–cancer population study. Aging 2023;15:13134–49.
26. Phinyo P, Jarupanich N, Lumkul L, Phanphaisarn A, Poosiripinyo T, Sukpanichyingyong S, et al. Validation of a diagnostic model to differentiate multiple myeloma from bone metastasis. Clin Epidemiol 2023;15:881–90.
27. Elsabah H, El Omri H, Habas E, Taha RY, ElKourashy SA, Ibrahim F, et al. Real world evidence of epidemiological trends, clinical presentation, and prognostic outcomes of multiple myeloma (2007–2021). Front Med 2024;11:1338552.
28. Sweet DE, Madewell JE, Ragsdale BD. Radiologic and pathologic analysis of solitary bone lesions. Part III: matrix patterns. Radiol Clin North Am 1981;19:785–814.
29. Daniel A, Ullah E, Wahab S, Kumar V. Relevance of MRI in prediction of malignancy of musculoskeletal system–A prospective evaluation. BMC Musculoskelet Disord 2009;10:125.
30. Alyas F, James SL, Davies AM, Saifuddin A. The role of MR imaging in the diagnostic characterisation of appendicular bone tumours and tumour–like conditions. Eur Radiol 2007;17:2675–86.
31. Zimmer WD, Berquist TH, McLeod RA, Sim FH, Pritchard DJ. Bone tumors: magnetic resonance imaging versus computed tomography. Radiology 1985;155:709–18.

32. Xu J, Hu Y, Zhou R, Sun S, Chen H. Zero echo time vs. T1-weighted MRI for assessment of cortical and medullary bone morphology abnormalities using CT as the reference standard. J Magn Reson Imaging 2023;58:752-60.